Eur. Phys. J. D (2014) 68: 125
DOI: 10.1140/epjd/e2014-50085-7

THE EUROPEAN PHYSICAL JOURNAL D

Regular Article

Electron swarm transport in THF and water mixtures*

Ronald D. White[1,a], Michael J. Brunger[2,3], Nathan A. Garland[1], Robert E. Robson[1], Kevin F. Ness[1], Gustavo Garcia[4], Jaime de Urquijo[5], Sasa Dujko[6], and Zoran Lj. Petrović[6]

[1] ARC Centre for Antimatter-Matter Studies, School of Engineering and Physical Sciences, James Cook University, 4810 Townsville, Australia
[2] ARC Centre for Antimatter-Matter Studies, School of Chemical and Physical Sciences, Flinders University, GPO Box 2100, SA 5001 Adelaide, Australia
[3] Institute of Mathematical Sciences, University of Malaya, 5063 Kuala Lumpur, Malaysia
[4] Instituto de Física Fundamental, Consejo Superior de Investigaciones Científicas, 28006 Madrid, Spain
[5] Instituto de Ciencias Físicas, Universidad Nacional Autónoma de México, 62251 Cuernavaca, Morelos, Mexico
[6] Institute of Physics, University of Belgrade, Pregrevica 118, 11080 Belgrade, Serbia

Received 30 January 2014 / Received in final form 24 February 2014
Published online 20 May 2014 –

Abstract. The transport coefficients of electrons in mixtures of gaseous water and tetrahydrofuran (THF) are calculated using a multi-term solution of the Boltzmann equation. Electron transport coefficients at room temperature are presented over a range of reduced electric fields from 0.1–1000 Td, with significant differences between the behaviour in pure water and pure THF being found. The influence of the water to THF mixture ratio on the calculated transport coefficients is also presented.

1 Introduction

An understanding of the interaction of electrons with human tissue is of importance in many fields ranging from imaging to dosimetry in medicine and therapy [1–3]. Treatments involving ionizing radiation liberate low-energy electrons (average energies of 20–30 eV), which subsequently interact and deposit energy in the biomolecules that constitute human tissue. Damage associated with such ionizing radiation has been attributed in part to the low-energy dissociative electron attachment (DEA) that induces single and double strand breaks in DNA, or indirectly through interaction of electron-induced radicals with DNA [1]. In plasma medicine, an understanding of the plasma-tissue interactions at the interface, including the electron-impact generation of radicals, and penetration of the plasma and associated fields into the tissue, is of key importance to a predictive understanding of plasma treatments using dielectric barrier discharges [3]. Fundamentally, an understanding of non-equilibrium electron-induced processes and interactions with biomolecules that constitute human tissue, namely water, the sugars and DNA bases, is one essential component required to accurately model these applications.

When applying GEANT4/PENELOPE or other kinetic modelling techniques, radiation scientists and plasma-tissue interface modellers often use *water vapour* (H_2O) as the default substance for studying effects in biological material [4–7]. In reality, biological media is not water vapour but rather a complex mixture of biological molecules in a soft-condensed phase, and so the open question is just how good an approximation this default position actually is.

On treatment of biological media as a gas, our recent program [8–10] has focused on the development of charged particle transport in soft-condensed matter. We have looked to adapt gas-phase cross-sections, introducing structure modified cross-sections (via measured static structure factors) which account for coherent scattering associated with the short-ranged structure in soft-condensed systems. Large differences have been shown to arise in the transport properties in the gas-phase as opposed to the soft-condensed phase [8–10].

On the use of water as the surrogate for biological media, recently, much effort has been focused on establishing complete and accurate sets of electron impact cross-sections for biomolecules. Two of the most complete sets for biomolecules exist for water and tetrahydrofuran (THF, C_4H_8O) – an excellent prototype for species that form DNA. For electron impact cross-sections in water, there have been a number of complete or nearly complete sets of cross-sections proposed [11–14]. For THF, a near-complete set of total, momentum transfer and integral cross sections describing its electron scattering behaviour has recently become available in the literature [15].

* Contribution to the Topical Issue "Electron and Positron Induced Processes", edited by Michael Brunger, Radu Campeanu, Masamitsu Hoshino, Oddur Ingólfsson, Paulo Limão-Vieira, Nigel Mason, Yasuyuki Nagashima and Hajime Tanuma.

[a] e-mail: ronald.white@jcu.edu.au

One of the key discriminating assessments of the accuracy and completeness of proposed cross-section sets is provided by swarm experiments [16–18]. For electrons in water vapour, experimentally measured swarm transport coefficients have been provided initially by the Australian and Japanese groups [19,20] and more recently by the Mexican group using the pulsed-Townsend technique [21]. The current authors have recently reviewed and refined the cross-section set for water through comparison of calculated data with measured swarm data [14,22]. Recent measurements of electron swarms in water and helium mixtures have enabled a further refinement of the cross-section set [23], and these have been implemented in the current study. Unfortunately there is currently no experimental swarm data available for THF, due to complications with its use in the drift tube at 300 K [15]. The recently proposed methodology for addressing those issues [15] is currently being implemented.

In this study we begin to address the question of the validity of a water vapour model for human tissue. Here, albeit initially in the gas phase, we compare the behaviour of the electron swarm transport coefficients in water and THF and their mixtures. In Section 2, we begin with a brief discussion of the calculation of electron swarm transport coefficients in mixtures using a multi-term solution of the Boltzmann equation. The variation of the swarm transport coefficients with density-reduced electric field, E/n_0, and mixture ratios are presented and discussed in Section 3. Conclusions drawn from the present investigation are detailed in Section 4.

2 Theory and simulation

In this study we use a multi-term solution of the Boltzmann equation to investigate the transport of electrons in mixtures of THF and water vapour. In the following sections we briefly discuss the techniques, but prefer to refer readers to the review in reference [24] for further details. Note that our multi-term Boltzmann equation solutions have been systematically benchmarked and validated against independent Monte-Carlo simulations for a variety of external field configurations and profiles [24].

2.1 The Boltzmann equation

The analysis of electron transport in gases can be treated semi-classically by solving the Boltzmann equation for the phase-space distribution function $f(\boldsymbol{r},\boldsymbol{c},t)$ [25]:

$$\frac{\partial f}{\partial t}+\boldsymbol{c}\cdot\nabla f+\frac{q\boldsymbol{E}}{m}\cdot\frac{\partial f}{\partial \boldsymbol{c}}=-J(f), \tag{1}$$

where $\boldsymbol{r}$ and $\boldsymbol{c}$ denote, respectively the position and velocity co-ordinates in phase space while q and m are the charge and mass of the particle respectively, and $\boldsymbol{E}$ is the applied external field. The right hand side of (1) represents the total collision operator J, describing the rate of change of the phase-space distribution function due to collisions between the swarm particles and the neutral background gas mixture molecules:

$$J\left(f,F_0\right)=\sum_i \alpha_i J\left(f,F_0^i\right), \tag{2}$$

where the sum is over the gases in the mixture and α_i represents the mole fraction of gas i. For elastic, inelastic and super elastic collisions are described by the Wang-Chang, Uhlenbeck, de Boer semi-classical collision operator [26], while electron attachment and ionisation operators are detailed in reference [27].

2.2 Transport coefficients

Charged particle currents or charged particle densities, $n(\boldsymbol{r},t)$, are generally sampled in swarm experiments. The connection between experiment and theory is usually made through the equation of continuity:

$$\frac{\partial n}{\partial t}+\nabla\cdot\boldsymbol{\Gamma}(\boldsymbol{r},t)=S(\boldsymbol{r},t), \tag{3}$$

where

$$n(\boldsymbol{r},t)=\int f(\boldsymbol{r},\boldsymbol{c},t)d\boldsymbol{c}, \tag{4}$$

while $\boldsymbol{\Gamma}(\boldsymbol{r},t)=n\langle\boldsymbol{c}\rangle$ is the swarm particle flux and $S(\boldsymbol{r},t)$ represents the production rate per unit volume per unit time arising from non-conservative collisional processes. Swarm experiments are carefully designed to operate in the hydrodynamic regime, where the space-time dependence of the phase-space distribution function is expressible in terms of the well-known density gradient expansion [22,27,28]:

$$f(\boldsymbol{r},\boldsymbol{c},t)=\sum_{k=0}^{\infty} f^{(k)}(\boldsymbol{c},t)\odot(-\nabla)^k n(\boldsymbol{r},t), \tag{5}$$

where $f^{(k)}(\boldsymbol{c},t)$ are time-dependent tensors of rank k and $\odot$ denotes a k-fold scalar product. Assuming the functional relationship in equation (5), the flux $\boldsymbol{\Gamma}(\boldsymbol{r},t)$ and source term $\boldsymbol{S}(\boldsymbol{r},t)$ in equation (3) are expanded as:

$$\boldsymbol{\Gamma}(\boldsymbol{r},t)=\boldsymbol{W}_F\, n(\boldsymbol{r},t)-\mathbf{D}_F\cdot\nabla n(\boldsymbol{r},t) \tag{6}$$

$$S(\boldsymbol{r},t)=S^{(0)}n(\boldsymbol{r},t)-\boldsymbol{S}^{(1)}\cdot\nabla n(\boldsymbol{r},t)+\mathbf{S}^{(2)}:\nabla\nabla n(\boldsymbol{r},t), \tag{7}$$

where $\boldsymbol{W}_F$ and $\mathbf{D}_F$ define, respectively the flux drift velocity and diffusion tensor. Substitution of expansions (6) and (7) into the continuity equation (3) yields the diffusion equation,

$$\frac{\partial n}{\partial t}+\boldsymbol{W}\cdot\nabla n-\mathbf{D}:\nabla\nabla n=-R_{net}(t)n, \tag{8}$$

which defines the bulk transport coefficients:

$$R_{net}=-S^{(0)} \tag{9}$$

$$\boldsymbol{W}=\boldsymbol{W}_F+\boldsymbol{S}^{(1)} \tag{10}$$

$$\mathbf{D}=\mathbf{D}_F+\mathbf{S}^{(2)}. \tag{11}$$

The coefficients that are measured in the various swarm experiments generally differ by (i) various treatments of the source term; and (ii) how they interpret the results of their experiments. Physically, the bulk transport coefficients are associated with the swarm's centre of mass transport (and spread about its centre of mass). The explicit influence of non-conservative collisional processes on the swarm's centre of mass transport is described by the terms $\boldsymbol{S}^{(1)}$ and $\mathbf{S}^{(2)}$. The two sets of transport coefficients (i.e. bulk and flux) coincide in the absence of non-conservative processes.

2.3 Multi-term solution of the Boltzmann equation

To solve the Boltzmann equation (1) in the hydrodynamic regime we make a series of representations of the various dependencies in $f(\boldsymbol{r}, \boldsymbol{c}, t)$. The angular dependence of the phase-space distribution function in velocity space can be represented in terms of an expansion in spherical harmonics:

$$f(\boldsymbol{r}, \boldsymbol{c}, t) = \sum_{l=0}^{\infty} \sum_{m=-l}^{l} f_m^{(l)}(\boldsymbol{r}, c, t) Y_m^{[l]}(\hat{\boldsymbol{c}}), \tag{12}$$

where $Y_m^{[l]}(\hat{\boldsymbol{c}})$ are spherical harmonics and $\hat{\boldsymbol{c}}$ denotes the angles of $\boldsymbol{c}$. This is a true multi-term treatment. Here we employ an expansion in speed space in terms of generalised Sonine $R_{\nu l}(\alpha c)$ polynomials [29]:

$$f_m^{(l)}(\boldsymbol{r}, c, t) = w(\alpha, c) \sum_{\nu=0}^{\infty} F_\alpha(\nu l m; \boldsymbol{r}, t) R_{\nu l}(\alpha c), \tag{13}$$

which are orthonormal with respect to a Maxwellian weight function $w(\alpha, c) = (\frac{\alpha^2}{2\pi})^{3/2} \exp\{\frac{-\alpha^2 c^2}{2}\}$, where $\alpha^2 = \frac{m}{kT_b}$. T_b is an arbitrary basis temperature used to optimize convergence.

Using spherical tensors, the density gradient expansion (5) takes the form [30]:

$$F_\alpha(\nu l m; \boldsymbol{r}, t) = \sum_{s=0}^{2} \sum_{\lambda=0}^{s} F(\nu l m | s\lambda) G_m^{(s\lambda)} n(\boldsymbol{r}, t), \tag{14}$$

where $G_m^{(s\lambda)}$ is the irreducible gradient tensor operator [30]. Performing the necessary operations, the following hierarchy of kinetic equations is obtained:

$$\sum_{\nu'=0}^{\infty} \sum_{l'=0}^{\infty} \Bigg[n_0 J_{\nu\nu'}^{l}(\alpha) \delta_{ll'} - R_{net} \delta_{\nu\nu'} \delta_{ll'} + i \frac{qE}{m} \alpha (l' m 10 | l m) \times \left\langle \nu l \left\| K^{[1]} \right\| \nu' l' \right\rangle - n_0 J_{0\nu'}^{0}(\alpha) F_\alpha(\nu l 0 | 00) \times (1 - \delta_{s0}\delta_{\lambda 0}) \delta_{l'0} \delta_{m0} \Bigg] F_\alpha(\nu' l' m | s\lambda) = \bar{X}(\nu l m | s\lambda; \alpha)$$
$$(\nu, l) = 0, 1, 2, \ldots, \infty, \; |m| \leq \min\{l, \lambda\}, \; s + \lambda = \text{even}, \tag{15}$$

where R_{net} is the net loss rate of charged particles and is defined in equation (16) below. The right hand side vectors for the required members of the hierarchy are given explicitly in reference [27], along with the reduced matrix elements of the velocity derivative $\langle \nu l || K^{[1]} || \nu' l' \rangle$ and collision operator $\langle \nu l m || J || \nu' l' m' \rangle = J_{\nu\nu'}^{l}(\alpha) \delta_{ll'} \delta_{mm'}$.

The transport coefficients of interest in the present study are then related to the calculated moments via:

$$R_{net} = n_0 \sum_{\nu'=0}^{\infty} J_{0\nu'}^{0}(\alpha) F_\alpha(\nu' 00 | 00), \tag{16}$$

$$W = \frac{i}{\alpha} F_\alpha(010|00) - i n_0 \sum_{\nu'=1}^{\infty} J_{0\nu'}^{0}(\alpha) F_\alpha(\nu' 00 | 11), \tag{17}$$

$$D_L = -\frac{1}{\alpha} F_\alpha(010|11) - n_0 \sum_{\nu'=1}^{\infty} J_{0\nu'}^{0}(\alpha) \times \left[F_\alpha(\nu' 00|20) - \sqrt{2} F_\alpha(\nu' 00|22) \right], \tag{18}$$

$$D_T = -\frac{1}{\alpha} F_\alpha(011|11) - n_0 \sum_{\nu'=1}^{\infty} J_{0\nu'}^{0}(\alpha) \times \left[F_\alpha(\nu' 00|20) + \frac{1}{\sqrt{2}} F_\alpha(\nu' 00|22) \right], \tag{19}$$

where the summations reflect the non-conservative corrections to the flux coefficients.

3 Results and discussion

3.1 Cross-section sets and inputs

The development of the complete cross-section set for water has been detailed in recent studies [14,22], and is based largely on the original set proposed in reference [11]. More recently, swarm data for mixtures of water and helium conducted using the accurate pulsed-Townsend technique [31], have enabled a revised set of momentum transfer cross-sections [23] to be used in the current study. The cross-section set employed here for water is displayed in Figure 1. The cross-section set for THF, displayed in Figure 2, has recently been proposed and detailed in reference [15]. We should note that thermally excited rotational state populations are considered for water (but not for THF) using Boltzmann statistics enabling superelastic rotational processes to be included. Note that in the present investigation we consider the density-reduced electric field (E/n_0) range from 0.1–1000 Td (1 Td = 10^{-21} V m^2). The background gas mixture temperature is fixed at 300 K.

3.2 Swarm transport

In Figures 3–7 we present our calculated transport coefficients for electrons in both pure THF and water, as well as various mixture ratios. Wherever possible, we have included experimental data for electron transport in water to support the validity of that cross-section set proposed.

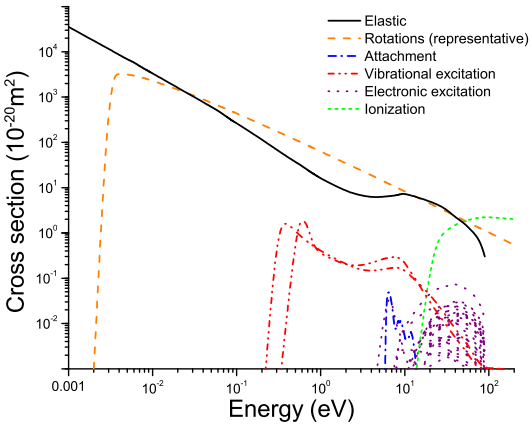

Fig. 1. Integral cross-section set for water largely based on the original set in reference [11] but updated to account for the more recent experimental data [14,23]. Anisotropic scattering is considered in the elastic and rotational cross-sections.

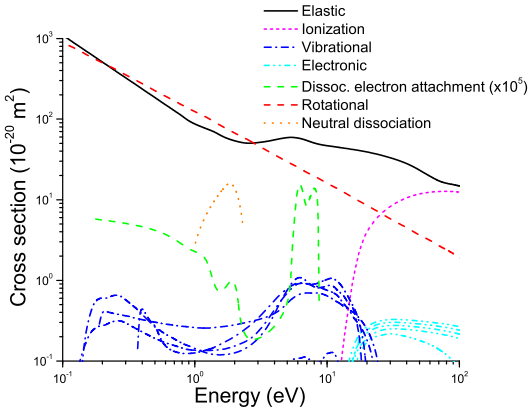

Fig. 2. Integral cross-section set for electrons in THF [15]. Anisotropic scattering was considered to the level of including the momentum transfer cross-section.

Errors in the two-term approximation were found to be as high as 80%, with an $l_{max} = 4$ sufficient to achieve convergence to within 1–2%, for the transport coefficients over the range of applied reduced fields considered.

Figure 3 displays the variation of the mean energy with THF/H_2O mixture ratio over a range of applied reduced fields. For fields up to 5 Td, both pure gases and their mixtures are caught in the thermal regime, where the mean energy is that of the background gas. The large rotational cross-sections for both gases (see Figs. 1 and 2) act to suppress deviations from thermal equilibrium. As the electric field is increased further, the thermal deadlock is broken first by THF. We should note that we have used a 'lumped' rotational cross-section for THF, with the cross-section having a representative threshold energy of 1.205 meV being implemented. In contrast, for water there are 120 rotational cross-sections considered in this study with an individual threshold for each process. The larger threshold energies, combined with the larger summed rotational cross-sections, result in the thermal deadlock for water remaining unbroken to higher fields. For pure water, we observe a rapid rise in the mean energy over a very short field range, indicative of a quasi-

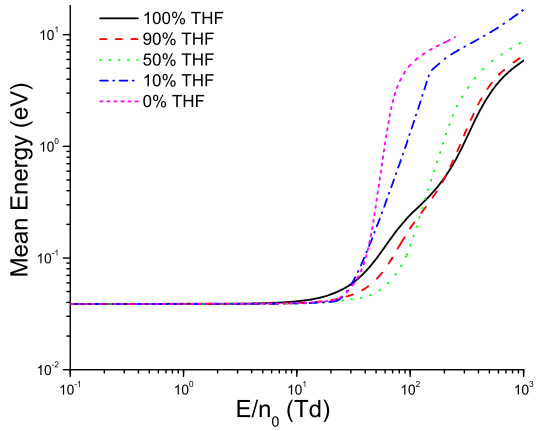

Fig. 3. Comparison of the calculated mean energies of electrons in THF-water mixtures, for varying fractions of THF. See legend in figure for further details.

runaway regime. At these fields, the swarm is sampling the rapidly falling component of the cross-sections in water. The quasi-runaway behaviour is eventually quenched by the opening of the vibrational channels in water and the rapid rate of increase in the swarm's mean energy then decreases [11,14]. Increasing the THF fraction, we note that this partial runaway regime is mitigated, and the rapid rise in the mean energy is now reduced. This is also reflected in the numerical solution of the Boltzmann equation: for the intermediate regime, convergence is very slow for pure water and we note that increasing the fraction of THF improves the convergence rate and the computational issues that exist with water are removed through the inclusion of THF in the background gas. At higher fields, ionization and electronic excitation processes become operative and the energy variation with the field is slowed for all mixture ratios considered. The mean energy appears to be a monotonically decreasing function of THF concentration in this regime.

In Figure 4 we display the variation of the density-normalized net particle creation rate arising from non-conservative processes including ionization, attachment and dissociative electron attachment. At low fields, for all mixtures including some fraction of THF, we observe the presence of the important dissociative electron attachment process. This DEA rate decreases in proportion with the decreasing THF fraction. For pure water we have attachment only at moderate fields, since the threshold for attachment is 5.6 eV. The attachment cross-section for water is greater than the DEA for THF, and dominates the profiles for mixtures in this intermediate field regime. The field at which there is a transition to an ionization-dominated regime varies with the mixture ratio. While the cross-section for ionization in water below 100 eV is in general lower than that for THF, the mean energy is generally higher at a given field for water than THF. It then follows that the ionization rate for water is higher than for the mixtures including THF over the field regime considered.

In Figure 5 we display the variation of the flux drift velocity with reduced electric field for various mixtures.

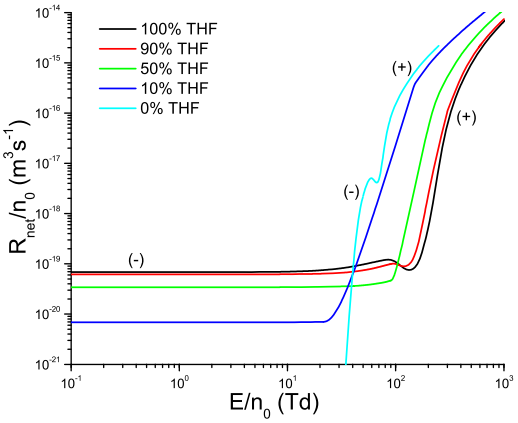

Fig. 4. Comparison of the calculated density-normalised net particle creation rates, R_{net}/n_0, for varying mixture ratios of THF to water. The $(-)$ and $(+)$ signs refer to the E/n_0 regions dominated by attachment and ionization, respectively. See legend in figure for further details.

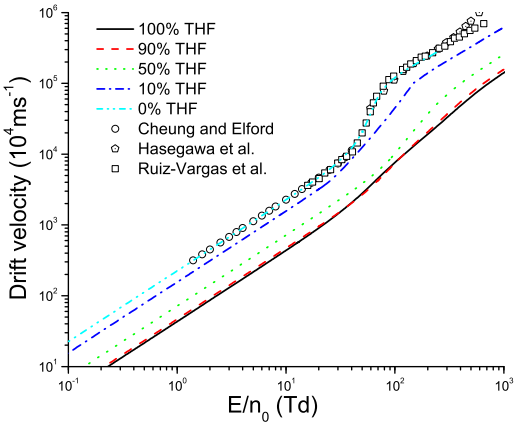

Fig. 5. Comparison of the flux drift velocities in varying THF-water fractions. The present results are compared with the experimental values for pure water vapour of Cheung and Elford [19], and the bulk-corrected results from Hasegawa et al. [20,22] and Ruiz-Vargas et al. [21]. See legend in figure for further details.

We also include the available experimental data for pure water vapour. In the thermal regime, the drift velocity is proportional to the field for all mixture ratios, as expected. The variation of the drift velocity with mixture ratio in this regime simply reflects the variation in the total momentum transfer cross-sections where we note that the momentum transfer cross-section for THF is much larger in magnitude than that for water vapour. This is further evidenced by the variation of the drift velocity in the 10% and 90% THF/H_2O profiles where one notes a proportionately bigger change with 10% inclusion of THF to water than there is for a 10% inclusion of water to THF. The mitigation of the partial runaway behaviour in water through the addition of THF is again displayed in the drift velocity. Finally, we draw the reader's attention to the suppression of the rapid increase in the drift velocity with field with increasing the THF fraction. Often Blanc's law is used to model mobility/drift velocities in mixtures [32].

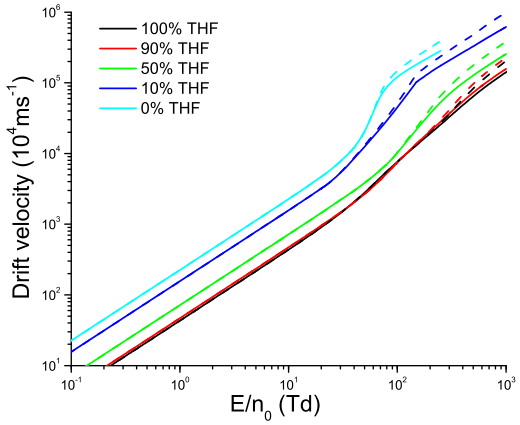

Fig. 6. Comparison of the bulk (dashed lines) and flux (solid lines) drift velocities calculated for varying mixture ratios of THF to water. See legend in figure for further details.

We note that the standard Blanc's law models the variation of the drift velocity with the mixture ratio accurately in the low field regime. At higher fields, however, as expected the accuracy of Blanc's law is reduced (though still qualitatively consistent) and one would need to employ the extended (common energy) version for improved accuracy [32].

In Figure 6 we display the bulk and flux drift velocities as a function of the reduced fields for various mixture ratios. At low fields there is essentially no difference between the two drift velocities, despite the presence of the non-conservative attachment process in both pure gases. The attachment rates are so low, however, that the centre-of-mass corrections brought about by attachment are not observable on this scale. When ionization becomes dominant, however, we note that the bulk drift velocity is always greater than the flux drift velocity. This follows since there is preferential ionization at the front of the swarm, and hence the particle generation at the front necessarily shifts the centre-of-mass in the direction of the drift. The bulk drift velocity enhancement over the flux drift velocity then follows. Depending on the type of swarm experiment and its analysis, one may measure either of these drift velocities. Generally it is the flux drift velocity that is measured in the pulsed-Townsend experiment, while it is it the bulk drift velocity that is measured in a time-of-flight experiment.

The variation of the diffusion coefficients with reduced fields, for the pure gases and a 50% THF/H_2O mixture are displayed in Figure 7. At low fields, the diffusion is isotropic ($n_0D_T \approx n_0D_L$), independent of the mixture ratio. In this regime, the thermal contribution to diffusion is the dominant source, and the isotropy in the diffusion then follows. As the thermal deadlock is broken, diffusion becomes anisotropic, with $n_0D_L > n_0D_T$ for both pure THF and water, and their mixtures. This is an electric-field induced anisotropy and arises by virtue of a spatial variation of the average energy through the swarm and an energy dependent collision frequency [33]. We note that for all fields, diffusion in water is greater than that in THF. This is reflective of the enhanced collision frequencies for THF

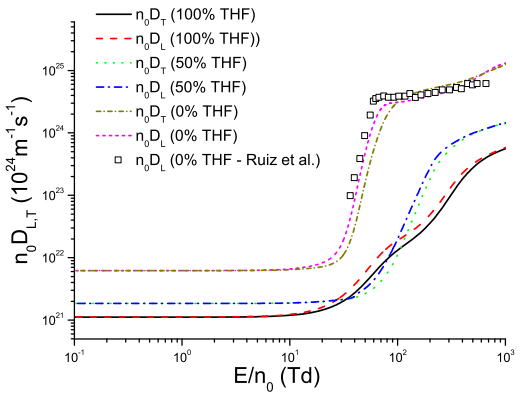

Fig. 7. Comparison of the flux longitudinal and transverse diffusion coefficients calculated for varying mixture ratios of THF to water. See legend in figure for further details.

as compared with water. This is further supported by the 50% THF/H_2O mixture results presented, where we note that these profiles lie closer to the THF profiles than those for water.

4 Concluding remarks

In this study we have began to address the question on the appropriateness of water-vapour as a surrogate for modelling electron induced processes in human tissue. As a first step, we have calculated transport coefficients in pure water vapour and THF, as well as for varying mixture ratios. We have found that the electron transport behaviour in water and in THF are distinctly different, and can in some cases have differences in their transport coefficients of an order of magnitude or more for a given electric field.

In reality, one needs to proceed beyond the gas phase model to include the soft-condensed nature of human tissue. This issue has been addressed in part through the adaptation of gas-phase cross-sections/interaction potentials to consider the spatio-temporal correlations that exist within the soft-condensed material [8–10]. Future efforts are focussed on extending this formalism to targets with long range dipole dominated interactions, that exist in the biomolecules, and orientational correlations present in biological media.

The authors would like to thank the Australian Research Council through its Centres of Excellence and Discovery programmes for financial support, the Australian Academy of Science through its European Scientific Exchange Program, Spanish Ministerio de Economia y Competitividad (Project FIS2012-31230) and MONTRS Projects ON171037 (and III41011). The experimental part was supported by Project PAPIIT IN 111014.

References

1. B. Boudaiffa, P. Cloutier, D. Hunting, M.A. Huels, L. Sanche, Science **287**, 1658 (2000)
2. S.R. Cherry, J.A. Sorensen, M.E. Phelps, *Physics in Nuclear Medicine* (Saunders Elsevier, Philadelphia, 2003)
3. D. Dobrynin, G. Fridman, G. Friedman, A. Fridman, New J. Phys. **11**, 115020 (2009)
4. C. Champion, Phys. Med. Biol. **48**, 2147 (2003)
5. H. Nikjoo, S. Uehara, D. Emfietzoglou, F. Cucinotta, Radiat. Meas. **41**, 1052 (2006)
6. Z. Francis, S. Incerti, M. Karamitros, H.N. Tran, C. Villagrasa, Nucl. Instrum. Methods Phys. Res. B **269**, 2307 (2011)
7. L.H. Toburen, Int. J. Rad. Biol. **88**, 2 (2012)
8. R.D. White, R.E. Robson, Phys. Rev. Lett. **102**, 230602 (2009)
9. R.D. White, R.E. Robson, Phys. Rev. E **84**, 1 (2011)
10. R.D. White, W. Tattersall, G. Boyle, R.E. Robson, S. Dujko, Z.Lj. Petrović, A. Banković, M.J. Brunger, J.P. Sullivan, S.J. Buckman, G. Garcia, Appl. Radiat. Isotopes **83**, 77 (2014)
11. K.F. Ness, R.E. Robson, Phys. Rev. A **38**, 1446 (1988)
12. M. Yousfi, M.D. Benabdessadok, J. Appl. Phys. **80**, 6619 (1996)
13. Y. Itikawa, N. Mason, J. Phys. Chem. Ref. Data **34**, 1 (2005)
14. K.F. Ness, R.E. Robson, M.J. Brunger, R.D. White, J. Chem. Phys. **136**, 024318 (2012)
15. N.A. Garland, M.J. Brunger, G. Garcia, J. de Urquijo, R.D. White, Phys. Rev. A **88**, 062712 (2013)
16. L.G.H. Huxley, R.W. Crompton, *The Drift and Diffusion of Electrons in Gases* (Wiley, New York, 1974)
17. Z.Lj. Petrović, M. Šuvakov, Z. Nikitović, S. Dujko, O. Šašić, J. Jovanović, G. Malović, V. Stojanović, Plasma Sources Sci. Technol. **16**, S1 (2007)
18. Z.Lj. Petrović, S. Dujko, D. Marić, G. Malović, Z. Nikitović, O. Šašić, J. Jovanović, V. Stojanović, M. Radmilović-Radjenović, J. Phys. D **42**, 194002 (2009)
19. B. Cheung, M.T. Elford, Aust. J. Phys. **43**, 755 (1990)
20. H. Hasegawa, H. Date, M. Shimozuma, J. Phys. D **40**, 2495 (2007)
21. G. Ruíz-Vargas, M. Yousfi, J. de Urquijo, J. Phys. D **43**, 455201 (2010)
22. R.E. Robson, R.D. White, K.F. Ness, J. Chem. Phys. **134**, 064319 (2011)
23. J. de Urquijo, E. Basurto, K.F. Ness, M.J. Brunger, R.D. White, Electron swarm transport coefficients in H_2O-He mixtures: Experiment and calculations (in preparation)
24. R.D. White, R.E. Robson, S. Dujko, P. Nicoletopoulos, B. Li, J. Phys. D **42**, 194001 (2009)
25. L. Boltzmann, Wein. Ber. **66**, 275 (1872)
26. C.S. Wang-Chang, G.E. Uhlenbeck, J. De Boer, in *Studies in Statistical Mechanics*, edited by J. De Boer, G.E. Uhlenbeck (Wiley, New York, 1964), Vol. II, p. 241
27. K.F. Ness, R.E. Robson, Phys. Rev. A **34**, 2185 (1986)
28. K. Kumar, H.R. Skullerud, R.E. Robson, Aust. J. Phys. **33**, 343 (1980)
29. S. Chapman, T.G. Cowling, *The Mathematical Theory of Non-Uniform Gases* (Cambridge University Press, Cambridge, 1939)
30. R.E. Robson, K.F. Ness, Phys. Rev. A **33**, 2068 (1986)
31. E. Basurto, J.L. Hernández-Ávila, A.M. Juárez, J. de Urquijo, J. Phys. D **46**, 355207 (2013)
32. J.V. Jovanović, S.B. Vrhovac, Z.Lj. Petrović, Eur. Phys. J. D **28**, 91 (2004)
33. R.D. White, R.E. Robson, K.F. Ness, Aust. J. Phys. **48**, 925 (1995)